

# ACPW Dual-Band Bandpass Filter with Independently Controllable Transmission Zeros

Zhongbao WANG, Shaojun FANG

School of Information Science and Technology, Dalian Maritime University, Dalian, Liaoning 116026, China

wangzb@dmlu.edu.cn, fangshj@dmlu.edu.cn

**Abstract.** Compact dual-band bandpass filters with stepped-impedance conductor-backed asymmetric coplanar waveguide resonators are proposed, and synthesis formulas are derived to facilitate the design. By using an asymmetric topology, two additional transmission zeros are obtained. To further improve the selectivity, an embedded coplanar waveguide resonator is proposed to achieve two independently controllable transmission zeros. Two dual-band bandpass filters are designed and fabricated. The measured results validate the proposed design.

## Keywords

Dual-band bandpass filter, asymmetric coplanar waveguide, asymmetric topology, embedded CPW resonator, independently controllable transmission zeros.

## 1. Introduction

Currently, dual-band bandpass filters (DBBPFs) are highly desired in modern wireless communication systems. To meet the need, some ingenious DBBPFs have been reported. In 1997, a DBBPF was first realized with parallel connection of different bandpass filters [1]. Then, many DBBPFs based on the concept have been developed by using two sets of independent resonators combined with common input and output ports [2-4]. In 2004, another type of DBBPFs was presented by using a wideband bandpass filter cascaded with a bandstop structure [5]. However, the size is very large [1-3], [5]. To reduce the size, the methods using stepped-impedance resonators (SIRs), dual-mode resonators and defected ground structures (DGS) have been reported in [6-12]. However, the design of these filters is conducted by the electromagnetic (EM) simulation which is inefficient. To improve the efficiency, a systematic synthesis method was presented for a DBBPF with controllable second passband in [13]. Based on the concept, flexible passband and bandwidth selections were achieved by replacing uniform-impedance resonators with SIRs [14]. The DBBPFs in [13], [14] has been a popular choice due to its relatively simple design procedure (closed-form design

formulas are available). However, the selectivity needs to be improved.

Usually, the selectivity can be enhanced by increasing poles, but the size is also increased. To solve this problem, cross-coupled filters have been proposed. In [15], coupling/shielding lines were presented to control the cross couplings for realizing two independently controllable transmission zeros. However, the synthesis of the coupling matrix is complex. Open stubs or spurlines were also used to improve the selectivity [7], [16]. However, the dimensions of the DBBPFs are needed to be adjusted for a good impedance matching in the passbands.

Many DBBPFs have been designed with microstrip lines. However, only few designs have used coplanar waveguides (CPWs) [17], [18], which are sensitive to environmental effects because their fields are less confined than those of microstrip lines. To solve this problem, conductor-backed CPWs have been proposed and widely used in microwave integrated circuits due to several attractive features, such as low radiation losses, less dispersion and easy integration with active devices. Conductor-backed asymmetric coplanar waveguides (ACPWs) provide additional degrees of freedom to control the line characteristic and optimize the circuit performance [19], [20].

In this paper, the conductor-backed ACPW is adopted to realize the DBBPF and an asymmetric topology is introduced to improve the selectivity and reduce the size. Furthermore, an embedded CPW resonator is proposed to obtain independently controllable transmission zeros for further improving the selectivity. Two DBBPFs operating at GSM and DCS bands (890-960 MHz and 1710-1880 MHz) are designed to validate the proposed method.

## 2. Filter Synthesis Formulas

Fig. 1 gives the equivalent circuit of the proposed DBBPF. Each dual-band resonator consists of two stepped-impedance open stubs, which are connected by an admittance inverter (i.e.,  $J$ -inverter). Assume that the central frequencies of the first and second passbands are  $f_1$  and  $f_2$ , respectively. The electrical lengths of the open stubs with respect to  $f_1$  are also shown in Fig. 1. The susceptance of

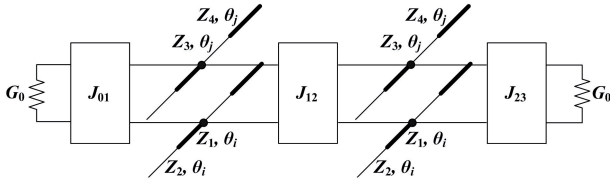


Fig. 1. Equivalent circuit of the proposed DBBPF.

the dual-band resonator is expressed by

$$B(f) = Y_1 \cdot \frac{(1 + R_i) \tan\left(\theta_i \frac{f}{f_1}\right)}{R_i - \tan^2\left(\theta_i \frac{f}{f_1}\right)} + Y_3 \cdot \frac{(1 + R_j) \tan\left(\theta_j \frac{f}{f_1}\right)}{R_j - \tan^2\left(\theta_j \frac{f}{f_1}\right)} \quad (1)$$

with  $Y_1 = 1/Z_1$ ,  $Y_3 = 1/Z_3$ ,  $R_i = Z_2/Z_1$ ,  $R_j = Z_4/Z_3$ . Then the susceptance slope parameter at its resonant frequency  $f_r$  can be obtained by

$$\beta_r = \frac{f_r}{2} \cdot \left. \frac{dB(f)}{df} \right|_{f=f_r} \quad (2)$$

The required slope parameters of the dual-band resonator at  $f_1$  and  $f_2$  are  $\beta_1$  and  $\beta_2$ , respectively. Assume that  $\alpha$  is the central frequency ratio (i.e.,  $\alpha = f_2/f_1$ ). The resonant conditions and slope parameters can be written as the following four equations:

$$B(f_1) = Y_1 \cdot \frac{(1 + R_i) \tan \theta_i}{R_i - \tan^2 \theta_i} + Y_3 \cdot \frac{(1 + R_j) \tan \theta_j}{R_j - \tan^2 \theta_j} = 0, \quad (3)$$

$$B(f_2) = Y_1 \cdot \frac{(1 + R_i) \tan(\alpha \theta_i)}{R_i - \tan^2(\alpha \theta_i)} + Y_3 \cdot \frac{(1 + R_j) \tan(\alpha \theta_j)}{R_j - \tan^2(\alpha \theta_j)} = 0, \quad (4)$$

$$\beta_1 = \frac{Y_1(1 + R_i)\theta_i \sec^2 \theta_i (R_i + \tan^2 \theta_i)}{2(R_i - \tan^2 \theta_i)^2} + \frac{Y_3(1 + R_j)\theta_j \sec^2 \theta_j (R_j + \tan^2 \theta_j)}{2(R_j - \tan^2 \theta_j)^2}, \quad (5)$$

$$\beta_2 = \frac{Y_1(1 + R_i)\alpha\theta_i \sec^2(\alpha\theta_i) [R_i + \tan^2(\alpha\theta_i)]}{2[R_i - \tan^2(\alpha\theta_i)]^2} + \frac{Y_3(1 + R_j)\alpha\theta_j \sec^2(\alpha\theta_j) [R_j + \tan^2(\alpha\theta_j)]}{2[R_j - \tan^2(\alpha\theta_j)]^2}. \quad (6)$$

Note that the central frequency ratio  $\alpha$  is given (for example,  $\alpha = f_2/f_1 = 1795/925 = 1.94$  for the GSM/DCS dual-band filter), and  $\beta_1$  and  $\beta_2$  are determined by the pass-band bandwidths. There are six unknowns ( $\theta_i$ ,  $\theta_j$ ,  $R_i$ ,  $R_j$ ,  $Y_1$  and  $Y_3$ ) but only four equations (3)-(6). This allows us to directly assign values to two variables. For example, the values of  $R_i$  and  $R_j$  can be freely adjusted to find practical values for the possible realization of  $\theta_i$ ,  $\theta_j$ ,  $Y_1$  and  $Y_3$ . Let  $\Delta_1$  and  $\Delta_2$  be the relative bandwidths at  $f_1$  and  $f_2$ , respectively. From the classical filter synthesis theory, we get that

$$J_{01} = \sqrt{\frac{G_0 \Delta_1 \beta_1}{g_0 g_1}}, \quad (t = 1, 2), \quad (7)$$

$$J_{23} = \sqrt{\frac{G_0 \Delta_2 \beta_2}{g_2 g_3}}, \quad (t = 1, 2), \quad (8)$$

where  $G_0$  is the termination conductance and  $g_i$  ( $i = 0, 1, 2, 3$ ) is the low-pass prototype value. Equations (7) and (8) are the same since  $g_0 g_1$  is equal to  $g_2 g_3$  for Butterworth and Chebyshev filters. Generally, to make the filter more compact, the admittance inverters ( $J_{01}$  and  $J_{23}$ ) at the input and output ports are chosen as  $J_{01} = J_{23} = G_0 = 0.02$  Siemens for  $50\Omega$  system so that they can be realized by using  $50\Omega$  TLs. Thus, we get that [13]

$$\beta_t = G_0 \frac{g_0 g_1}{\Delta_t}, \quad (t = 1, 2). \quad (9)$$

Here we use same resonators at each stage and equal values of admittance inverters at the first and second passbands to simplify the filter design. Then, the admittance inverters between the resonators are determined by [13]

$$J_{12} = \Delta_1 \frac{\beta_1}{\sqrt{g_1 g_2}} = \Delta_2 \frac{\beta_2}{\sqrt{g_1 g_2}}. \quad (10)$$

In [13], a transmission line (TL) shunted with open stubs at its ends was presented as a dual-band admittance inverter. Note that the open stubs can be merged into the open stubs of the dual-band resonators for a compact filter structure [13]. The characteristic impedance  $Z_a$  and electrical length  $\theta_a$  of the TL are calculated by

$$Z_a = \frac{1}{J_{12} \sin \theta_a}, \quad (11)$$

$$\theta_a = \frac{\pi}{\alpha + 1}. \quad (12)$$

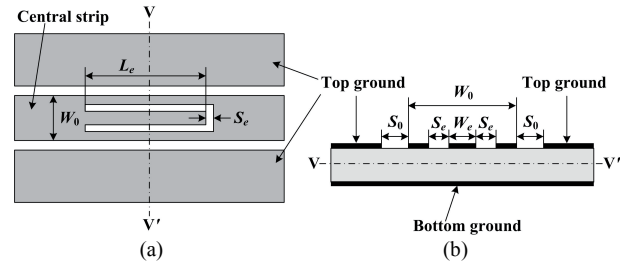


Fig. 2. Layout of embedded CPW resonator: (a) top view, (b) cross-sectional view.

### 3. Embedded CPW Resonator

It is well-known that a  $\lambda/4$  open stub can be used to realize a transmission zero. However, the impedance characteristic of the shunted TL is changed as a result of poor return losses in the passbands [16]. To reduce the effect of the open stub, we propose that the open stub is embedded in the central conductor strip of the  $50\Omega$  CPW as shown in Fig. 2. The simulated performances of the embedded CPW resonator with  $W_c = 0.5$  mm,  $S_g = 0.3$  mm,  $W_0 = 2.44$  mm, and  $S_0 = 1.0$  mm are given in Fig. 3. It is

seen that the stopband frequency increases with the decrease of  $L_e$ , which is the length of the open stub. The return losses at 925 and 1795 MHz are more than 20 dB when  $32 \text{ mm} \leq L_e \leq 38 \text{ mm}$ . Therefore, the application of the embedded CPW resonator to the DBBPF operating at 925 and 1795 MHz will have small effect on the passband performances when  $32 \text{ mm} \leq L_e \leq 38 \text{ mm}$ .

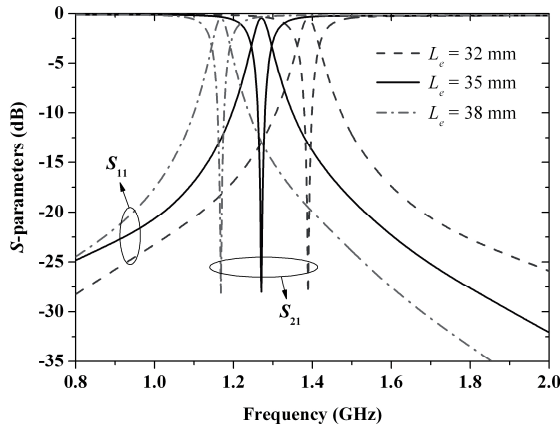


Fig. 3. Performances of the embedded CPW resonator.

### 4. Layout and Implementation

Fig. 4(a) gives the layout of the DBBPF with stepped-impedance conductor-backed ACPW resonators. Four 90° bends and an asymmetric topology are introduced to reduce the size. By using the asymmetric topology, two additional transmission zeros can be obtained, which will be proved in Section 5. Furthermore, the ground planes of conductor-backed ACPWs are connected to each other using via holes

in order to avoid the generation of undesired waveguide modes.

As an example, a two-pole Chebyshev DBBPF operating at GSM and DCS bands is designed and implemented with a 1.524 mm-thick Rogers TMM-4 substrate with a dielectric constant of 4.5. The filter has a ripple of 0.05 dB and equal ripple bandwidths of 8.6% at 925 MHz and 9.5% at 1795 MHz. From the classical filter synthesis theory [21], the Chebyshev low-pass prototype values are  $g_0 = 1$ ,  $g_1 = 0.6923$ ,  $g_2 = 0.5585$  and  $g_3 = 1.2396$ . By using the formulas given in Section 2, we get  $Z_1 = 60.00 \Omega$ ,  $Z_2 = 69.58 \Omega$ ,  $Z_3 = 60.00 \Omega$ ,  $Z_4 = 59.64 \Omega$ ,  $Z_a = 51.24 \Omega$ ,  $\theta_a = 61.21^\circ$ ,  $\theta_i = 59.12^\circ$  and  $\theta_j = 32.73^\circ$ . However, optimal electrical parameters of TLs must take account of the distributed capacitance effect of the open stubs at the ends. Therefore, the Advanced Design System (ADS) circuit simulator is used to optimize the electrical parameters of TLs with gradient optimization, the details of which including the optimization variables and goals are shown in Fig. 4(b). After optimization, the electrical parameters of TLs are  $Z_1 = 59.00 \Omega$ ,  $Z_2 = 47.50 \Omega$ ,  $Z_3 = 65.55 \Omega$ ,  $Z_4 = 51.07 \Omega$ ,  $Z_a = 52.88 \Omega$ ,  $\theta_a = 61.48^\circ$ ,  $\theta_i = 56.94^\circ$  and  $\theta_j = 31.13^\circ$ . Then using the ACPW synthesis model presented in [19], the physical dimensions are calculated. Also, the optimal dimensions must take the discontinuous interface into consideration, and the final dimensions are obtained by using HFSS EM software (version 11.0) with parametric sweep analysis for a good performance. Thus, the final dimensions are found and implemented as follows:  $L_1 = 30.0 \text{ mm}$ ,  $L_2 = 32.8 \text{ mm}$ ,  $L_3 = 15.3 \text{ mm}$ ,  $L_4 = 17.6 \text{ mm}$ ,  $L_a = 30.1 \text{ mm}$ ,  $L_{o1} = 8.0 \text{ mm}$ ,  $L_{o2} = 5.0 \text{ mm}$ , and the strip and slot widths of ACPWs are given in Tab. 1. The photograph of the fabricated DBBPF with stepped-impedance

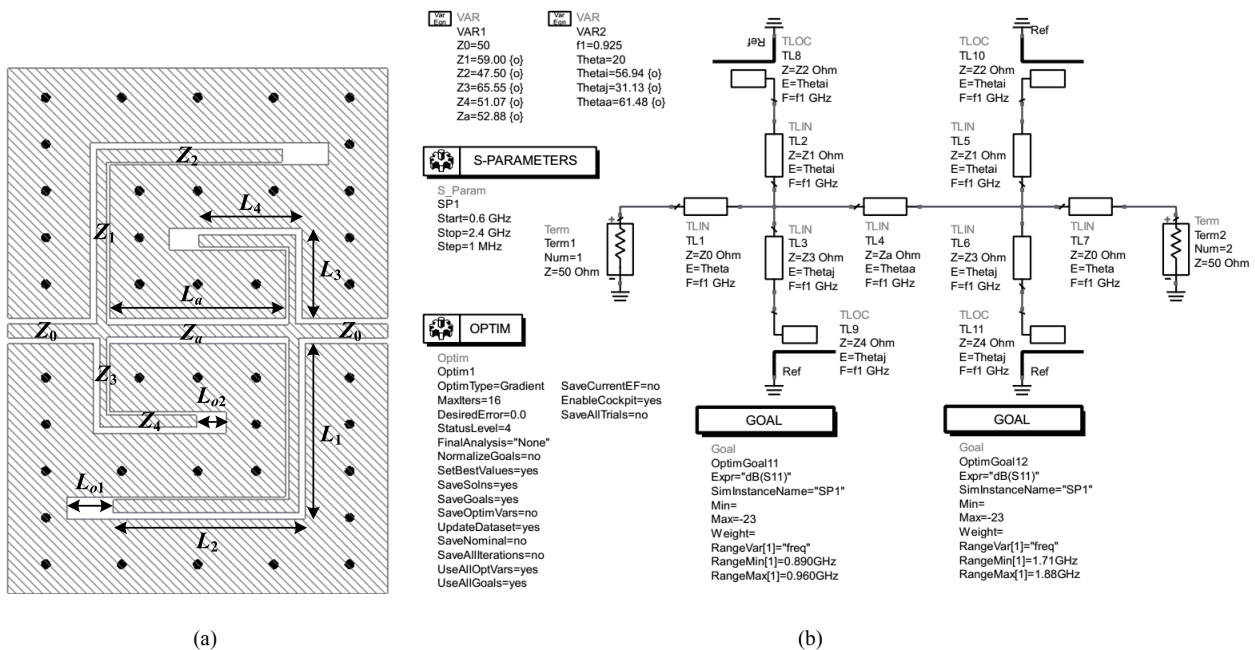


Fig. 4. a) Layout of DBBPF with stepped-impedance conductor-backed ACPW resonators. b) Simulation and optimization of the DBBPF in ADS2005 circuit simulator

conductor-backed ACPW resonators is shown in Fig. 5. The filter has the size of  $60 \text{ mm} \times 95 \text{ mm}$  (around  $0.32\lambda_g \times 0.51\lambda_g$ , where  $\lambda_g$  is the guided wavelength at the center frequency of the lower passband).

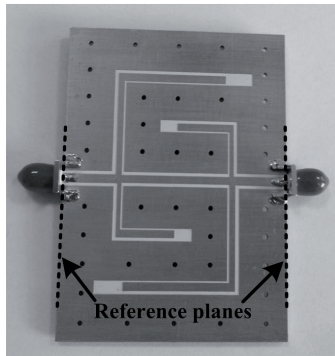


Fig. 5. Photograph of DBBPF with stepped-impedance conductor-backed ACPW resonators.

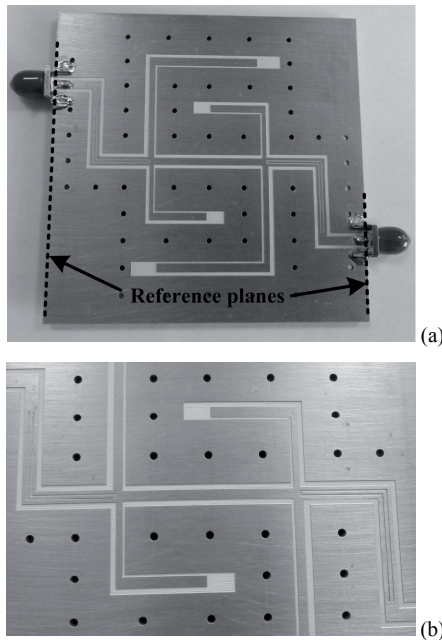


Fig. 6. DBBPF with stepped-impedance conductor-backed ACPW resonators and embedded CPW resonators: (a) whole view, (b) partially enlarged view.

Characteristic impedance	Strip width $W$ (mm)	Slot width	
		$S_1$ (mm)	$S_2$ (mm)
$Z_0$	2.44	1.00	1.00
$Z_1$	1.70	1.10	0.60
$Z_2$	2.30	1.00	0.50
$Z_3$	1.20	1.00	0.50
$Z_4$	2.10	1.00	0.50
$Z_a$	2.15	1.00	1.00

Tab. 1. Strip and slot widths of ACPWs.

To further improve the selectivity, two embedded CPW resonators with different  $L_e$  are inserted into the input and output ports of the DBBPF to add two transmission

zeros, as shown in Fig. 6. To reduce the effect of the embedded CPW resonators on the GSM and DCS bands,  $L_e$  is chosen to be 33 and 37 mm at input and output ports, respectively. Finally, the size of the DBBPF with stepped-impedance conductor-backed ACPW resonators and embedded CPW resonators is  $95 \text{ mm} \times 95 \text{ mm}$  (around  $0.51\lambda_g \times 0.51\lambda_g$ ).

## 5. Filter Performance

To validate the designs,  $S$ -parameters of the fabricated filters were measured with an Agilent PNA N5230A network analyzer setting the intermediate frequency bandwidth of 100 kHz. An 85052D 3.5mm thru-reflect-line (TRL) calibration kit was used to de-embed the filter's  $S$ -parameters from the measured data.

Fig. 7 gives the simulated and measured results of the DBBPF with stepped-impedance conductor-backed ACPW resonators. There is a good agreement between EM simulation and measurement. From the comparison between the circuit simulation and EM simulation, two additional transmission zeros are obtained by using the asymmetric topology. This is probably due to the interaction of electromagnetic fields between two open stubs located at the same side (above or below) of the TL with characteristic impedance  $Z_a$ . It is also seen from Fig. 6 that the measured stopband attenuation of the DBBPF near the transmission zeros is more than 50 dB, which reveals a 20 dB improvement in comparison with the DBBPF in [2], [6], [10], [14]. The measured return and insertion losses of both passbands are better than 19 dB and 0.4 dB, respectively, which are better than the existing DBBPFs [1-14]. This attributes to the use of conductor-backed ACPWs, the radiation loss of that is much smaller than the microstrip line [20].

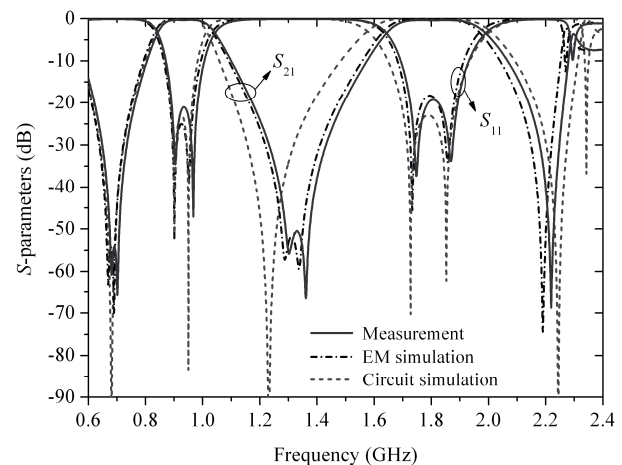
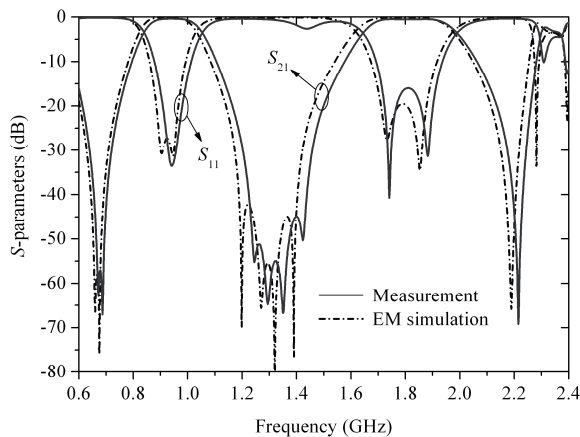


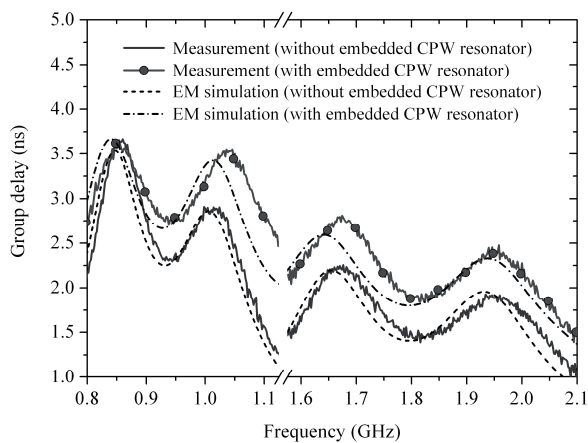
Fig. 7. Simulated and measured  $S$ -parameters of DBBPF with stepped-impedance conductor-backed ACPW resonators.

Fig. 8 shows the performances of the DBBPF with stepped-impedance conductor-backed ACPW resonators and embedded CPW resonators. Compared with the foregoing DBBPF, two transmission zeros at 1245 and

1423 MHz are achieved by adding embedded CPW resonators. Finally, a high selectivity DBBPF with seven transmission zeros are obtained. Furthermore, the measured return and insertion losses of both passbands are better than 16 dB and 0.55 dB, respectively, which mean that the effect of the embedded CPW resonator on the passband performance is less than that of spurlines [16]. Some deviation between the simulated and measured results is observed, which is mainly due to fabrication tolerance.



**Fig. 8.** Simulated and measured  $S$ -parameters of the DBBPF with stepped-impedance conductor-backed ACPW resonators and embedded CPW resonators.



**Fig. 9.** Simulated and measured group delay of the proposed DBBPFs.

Fig. 9 shows the simulated and measured group delays of the proposed DBBPFs when the reference planes are chosen as shown in Figs. 5 and 6. The measured group delay of the DBBPF with stepped-impedance conductor-backed ACPW resonators are 2.38 ns at 925 MHz with a variation within 0.70 ns for the first passband and 1.51 ns at 1795 MHz with a variation within 0.56 ns for the second passband. The variations against frequency for both passbands are similar to those of the DBBPF in [22]. It is also seen from Fig. 9 that the measured group delay of the DBBPF with stepped-impedance conductor-backed ACPW resonators and embedded CPW resonators are 2.83 ns at 925 MHz with a variation within 0.51 ns for the first pass-

band, and 1.95 ns at 1795 MHz with a variation within 0.69 ns for the second passband.

## 6. Conclusion

Compact DBBPFs with stepped-impedance conductor backed ACPW resonators are presented and synthesis formulas are derived to estimate the electrical parameters of TLs. Using the proposed asymmetric topology and embedded CPW resonators, a high selectivity DBBPF with seven transmission zeros including two independently controllable transmission zeros are realized. Two DBBPFs are designed and measured. The measured results show that stopband attenuation and passband matching of the proposed DBBPF are better than the existing DBBPF [2], [6], [10], [14].

## Acknowledgements

This work was supported jointly by the National Natural Science Foundation of China (No. 61071044), the Traffic Applied Basic Research Project of the Ministry of Transport of China (No. 2010-329-225-030), the Fundamental Research Funds for the Central Universities (No. 3132013053 and 3132013307) and the National Key Technologies R&D Program of China (No. 2012BAH36B01).

## References

- [1] MIYAKE, H., KITAZAWA, S., ISHIZAKI, T., YAMADA, T., NAGATOMI, Y. A miniaturized monolithic dual band filter using ceramic lamination technique for dual mode portable telephones. In *IEEE MTT-S International Microwave Symposium Digest*, Denver (USA), 1997, p. 789-792.
- [2] CHEN, C.-Y., HSU, C.-Y. A simple and effective method for microstrip dual-band filters design. *IEEE Microwave and Wireless Components Letters*, 2006, vol. 16, no. 3, p. 246-248.
- [3] WENG, M.-H., HUANG, C.-Y., WU, H.-W., SHU, K., SU, Y. K. Compact dual-band bandpass filter with enhanced feed coupling structures. *Microwave and Optical Technology Letters*, 2007, vol. 49, no. 1, p. 171-173.
- [4] CHEN, J.-X., YUM, T. Y., LI, J.-L., XUE, Q. Dual-mode dual-band bandpass filter using stacked-loop structure. *IEEE Microwave and Wireless Components Letters*, 2006, vol. 16, no. 9, p. 502-504.
- [5] TSAI, L. C., HUSE, C. W. Dual-band bandpass filters using equal-length coupled-serial-shunted lines and z-transform technique. *IEEE Transactions on Microwave Theory and Techniques*, 2004, vol. 52, no. 4, p. 1111-1117.
- [6] SUN, S., ZHU, L. Compact dual-band microstrip bandpass filter without external feeds. *IEEE Microwave and Wireless Components Letters*, 2005, vol. 15, no. 10, p. 644-646.
- [7] ZHANG, X. Y., CHEN, J.-X., SHI, J., XUE, Q. High-selectivity dual-band bandpass filter using asymmetric stepped-impedance resonators. *Electronics Letters*, 2009, vol. 45, no. 1, p. 63-64.

- [8] CHEN, Z.-X., DAI, X.-W., LIANG, C.-H. Novel dual-mode dual-band bandpass filter using double square-loop structure. *Progress in Electromagnetics Research*, 2007, vol. 77, p. 409-416.
- [9] ZHANG, R., ZHU, L., LUO, S. Dual-mode dual-band bandpass filter using a single slotted circular patch resonator. *IEEE Microwave and Wireless Components Letters*, 2012, vol. 22, no. 5, p. 233-235.
- [10] AHMED, E. S. Dual-mode dual-band microstrip bandpass filter based on fourth iteration T-square fractal and shorting pin. *Radioengineering*, 2012, vol. 21, no. 2, p. 617-623.
- [11] WU, B., LIANG, C.-H., QIN, P.-Y., LI, Q. Compact dual-band filter using defected stepped impedance resonator. *IEEE Microwave and Wireless Components Letters*, 2008, vol. 18, no. 10, p. 674-676.
- [12] WANG, L., GUAN, B.-R. Novel compact and high selectivity dual-band BPF with wide stopband. *Radioengineering*, 2012, vol. 21, no. 1, p. 492-495.
- [13] TSAI, C. M., LEE, H.-M., TSAI, C.-C. Planar filter design with fully controllable second passband. *IEEE Transactions on Microwave Theory and Techniques*, 2005, vol. 53, no. 11, p. 3429 to 3439.
- [14] GUAN, X., MA, Z., CAI, P., ANADA, T., HAGIWARA, G. Design of microstrip dual-band bandpass filter with controllable bandwidth. *Microwave and Optical Technology Letters*, 2007, vol. 49, no. 3, p. 740-742.
- [15] LIAO, C. K., CHANG, C. Y. Modified parallel-coupled filter with two independently controllable upper stopband transmission zeros. *IEEE Microwave and Wireless Components Letters*, 2005, vol. 15, no. 12, p. 841-843.
- [16] ZHANG, X. Y., CHEN, J.-X., XUE, Q., LI, S.-M. Dual-band bandpass filters using stub-loaded resonators. *IEEE Microwave and Wireless Components Letters*, 2007, vol. 17, no. 8, p. 583-585.
- [17] MAO, S.-G., WU, M.-S., CHUEH, Y.-Z. Design of composite right/left-handed coplanar-waveguide bandpass and dual-passband filters. *IEEE Transactions on Microwave Theory and Techniques*, 2006, vol. 54, no. 9, p. 3543-3549.
- [18] MAO, S.-G., CHUEH, Y.-Z., WU, M.-S. Asymmetric dual-passband coplanar waveguide filters using periodic composite right/left-handed and quarter-wavelength stubs. *IEEE Microwave and Wireless Components Letters*, 2007, vol. 17, no. 6, p. 418-420.
- [19] WANG, Z., FANG, S., FU, S. ANN synthesis models trained with modified GA-LM algorithm for ACPWs with conductor backing and substrate overlaying. *ETRI Journal*, 2012, vol. 34, no. 5, p. 696-705.
- [20] WANG, Z., FANG, S., FU, S., JIA, S. An inmarsat BGAN terminal patch antenna array with unequal input impedance elements and conductor-backed ACPW series-feed network. *IEEE Transactions on Antennas and Propagation*, 2012, vol. 60, no. 3, p. 1642-1647.
- [21] MATTHAEI, G. L., YOUNG, L., JONES, E. M. T. *Microwave Filter, Impedance-Matching Networks, and Coupling Structures*. Norwood: Artech House, 1980.
- [22] CAO, Q., WANG, G., LI, S. Design of dual-band bandpass filters using H-shaped resonators. *IET Microwaves, Antennas and Propagation*, 2012, vol. 6, no. 8, p. 915-921.

## About Authors ...

**Zhongbao WANG** was born in Sichuan province, China. He received his PhD in Communication and Information Systems from Dalian Maritime University (DLMU), China, in 2012. He is currently a lecturer in the School of Information Science and Technology, DLMU. His current research interests include passive RF components, patch antennas and microwave technology using artificial intelligence. He has authored or co-authored more than 20 papers in journals and conferences. He is currently serving as a technical reviewer for the IEEE Trans. on MTT, ETRI Journal and JMOe. He was the recipient of the Best Master's Thesis Award of Liaoning Province in 2009.

**Shaojun FANG** was born in Shandong province, China. He received his PhD in Communication and Information Systems from Dalian Maritime University (DLMU), China, in 2001. Since 1982, he has been working at DLMU, where he is currently a head professor in the School of Information Science and Technology. His recent research interests include passive RF components, patch antennas and computational electromagnetics. He has authored or coauthored three books and over 80 journal and conference papers. He is a member of the Editorial Board of the Chinese Journal of Radio Science and currently serving as a technical reviewer for the PIER/JEMWA Journals, Chinese Journal of Electronics, Journal of Systems Engineering and Electronics, and so on. He was the recipient of the Best Doctor's Dissertation Award of Liaoning Province in 2002 and the Outstanding Teacher Award of the Ministry of Transport of China.